# Incline Unbalanced Magnetic Pull Induced by Misalignment Rotor in PMSM

Yinquan Yu[1], Chao Bi[1], Phyu Nu Hla[1], Quan Jiang[1], Song Lin[1], Nay Lin Htun Aung[1], and Abdullah Al Mamun[2]

[1]Datastorage Institute, A-STAR, Singapore
[2]Department of Electrical and Computer Engineering, National University of Singapore, Singapore

**This paper analyzes the incline unbalanced magnetic pull (IUMP) generated in the permanent magnetic synchronous motor (PMSM) with the rotor misalignment. The motor magnetic field in such a motor is asymmetric, and both the magnitude and the action point of UMP vary in motor operation. This paper presents an analytical model for analyzing the 3-D effects of the UMP induced by the misalignment rotor. The numerical simulation results prove the effectiveness of the proposed analytic model.**

***Index Terms*— Incline unbalanced magnetic pull (IUMP), magnetic motive force (MMF), misalignment, permanent magnetic synchronous motor (PMSM).**

## I. Introduction

THE spindle motor used in hard disk drives (HDD) is a typical outer rotor permanent magnetic synchronous motor (PMSM), as shown in Fig. 1; it uses one end in a fixed fluid dynamic bearing (FDB) structure, resembling a slender cantilever beam, to support the rotor. Another PM motor structure is the inner rotor motor shown in Fig. 2. Both types of structures would generate uneven axial unbalanced magnetic pull (UMP) if there exists a misalignment of the rotor. The UMP is one of the sources that could produce the repeatable run-out (RRO) and nonrepeatable run-out (NRRO) in the motor. Therefore, the influence of the UMP is of great concern to the next generation of HDD with ultra-high area density.

The UMP affected by the drive mode and current was discussed in [1] and [2], and it will not be discussed in this paper. The UMP caused by mechanical tolerance can be divided into three types—dynamic UMP, static UMP, and incline UMP—which is caused by rotor uneven misalignment in axial direction. In previous work, most of the research was focused on dynamic UMP analysis [3]–[5]; some work covers the static UMP [6], but no detailed research exists for the IUMP. In this paper, the detailed analysis will be concentrated on the incline UMP (IUMP).

Normally, to improve the motor efficiency and power density, the motor air-gap should be as small as possible. However, the smaller the air-gap is, the more serious the rotor eccentricity will become, and thus the stronger the UMP will be. Besides HDD application, many PMSMs use self-alignment bearing [7], shown in Fig. 3, for reducing the rotor-bending force. It is clear that this kind of bearing could worsen the misalignment of the rotor, and consequently stronger IUMP could be induced.

There are many kinds of PMSM motors [8], [9]. In this paper, the analysis will be focused on the motors with surface PM ring

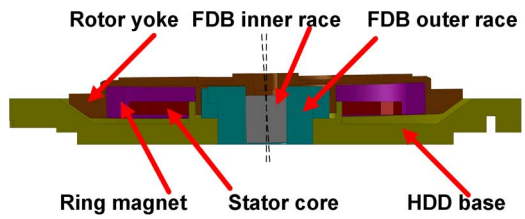


Fig. 1. Startup condition of spindle motor with FDB in hard disk.

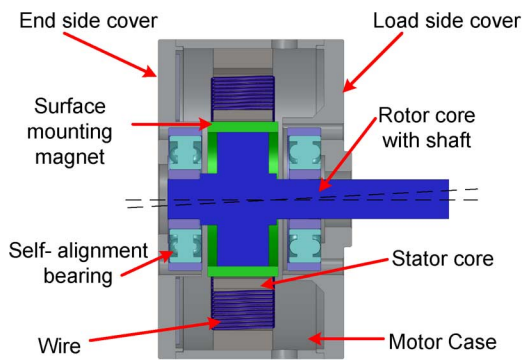


Fig. 2. Inner rotor PM-BLDC motor with self-alignment bearing.

on inner rotor shown in Fig. 2. This kind of motor is widely used in low power applications. Figs. 4–6 show the simplified electromagnetic (EM) models of PMSM with different types of axial misalignment rotors, respectively. In the following analysis, it is assumed that the permeability of the rotor yoke and stator core are infinite and the axial misalignment angles shown in Figs. 4–6 are assumed to be small values. Fig. 4 shows both ends of the rotor magnet center are misaligned in the same direction with respect to (w.r.t.) the center axis of stator core. In Fig. 5, only the right end of the rotor center is misaligned w.r.t. the center axis of stator core. Fig. 6 shows the left end of the rotor is downwardly misaligned while the right end is upwardly misalignment. Only the UMP shown in Figs. 4–6 will be studied in this paper. Moreover, the UMP caused by such misalignments may contain components in radial x, y and axial z directions, but only its component in radial x, y direction is considered in this paper.

Manuscript received November 30, 2012; revised February 01, 2013; accepted February 01, 2013. Date of current version May 30, 2013. Corresponding author: Y. Yu (e-mail: Yu_YinQuan@dsi.a-star.edu.sg).

Color versions of one or more of the figures in this paper are available online at http://ieeexplore.ieee.org.

Digital Object Identifier 10.1109/TMAG.2013.2245878

0018-9464/$31.00 © 2013 IEEE

Authorized licensed use limited to: University of Shanghai For Science and Technology. Downloaded on July 13,2020 at 12:10:12 UTC from IEEE Xplore. Restrictions apply.

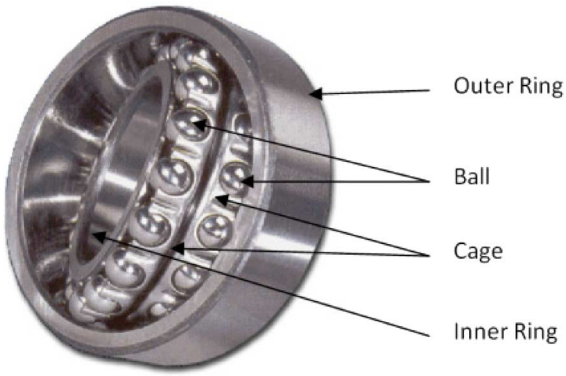


Fig. 3. Self-alignment bearing using in PM-BLDC motor operation [7].

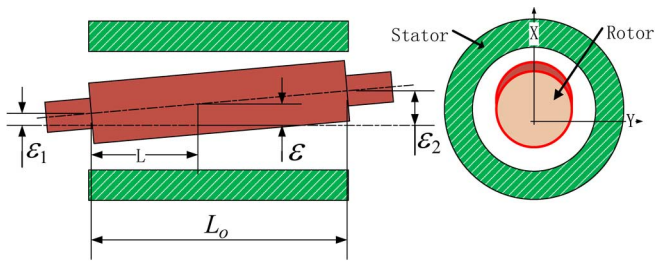


Fig. 4. PMSM with two ends of rotor upward from stator center with different distance.

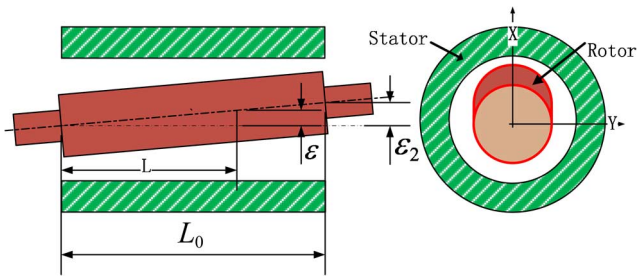


Fig. 5. PMSM with one end of rotor upward from stator center.

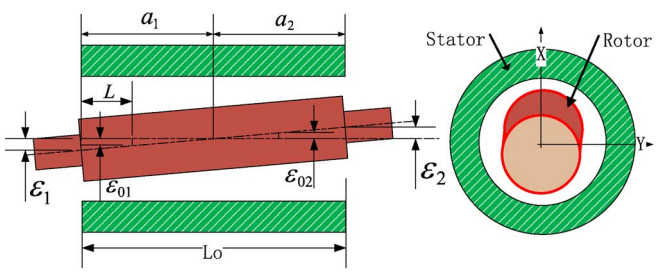


Fig. 6. PMSM with one end of rotor upward from stator center and another end of rotor downward from stator center.

## II. IUMP Characteristics in Space Domain

One cross section of the motor was taken as in Fig. 7, and the stator geometry can be expressed as

$$[P(\theta,\alpha,\delta)\cos(\theta-\alpha+\delta)+e]^2 + [P(\theta,\alpha,\delta)\sin(\theta-\alpha+\delta)]^2 = R^2 \quad (1)$$

where $x_0, y_0$ are the rotor center coordinates, $e$ the distance between rotor center and stator center, $r$ the outer diameter of rotor,

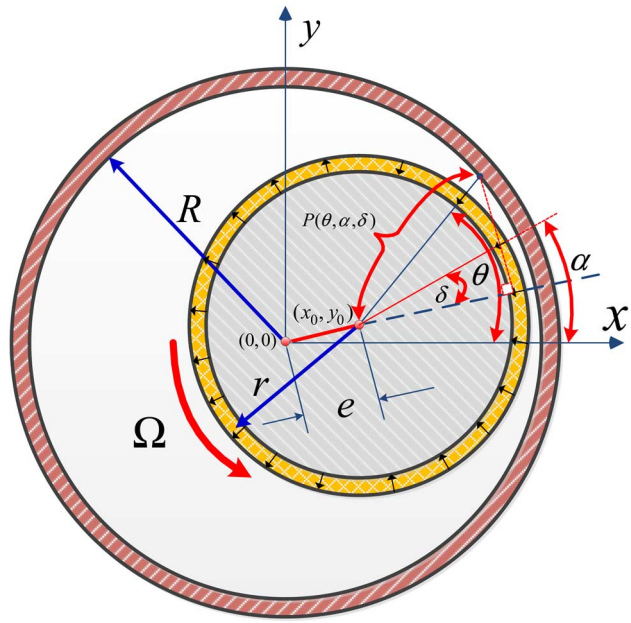


Fig. 7. Mathematics model for calculating uneven air-gap.

$R$ the inner diameter of stator, $\alpha$ the rotor position in stator coordinate, and $\delta$ the phase difference between the eccentric position and rotor position. $P(\theta,\alpha,\delta)$ can thus be deduced as

$$P(\theta,\alpha,\delta) = -e\cos(\theta-\alpha+\delta) \pm \sqrt{R^2+e^2\left[\sin(\theta-\alpha+\delta)\right]^2}. \quad (2)$$

From Fig. 7, it can be known that $P(\theta,\alpha,\sigma)>0$ and $e\sin(\theta-\alpha+\delta)/R \ll 1$. Therefore, (2) can be deduced as

$$P(\theta,\alpha,\delta) = R - e\cos(\theta-\alpha+\delta). \quad (3)$$

The eccentricity air-gap in the cross section can be expressed as

$$\delta_{\theta,\alpha,\delta} = P(\theta,\alpha,\delta) - r = \delta_0\left[1-\varepsilon\cos(\theta-\alpha+\delta)\right] \quad (4)$$

where $\delta_0$ is the average air-gap and $\varepsilon$ the relative eccentricity. The unit permeance of motor air-gap can be expressed as

$$\Lambda_e\theta,\alpha,\delta = \frac{\mu_0}{k_\mu\delta_{\theta,\alpha,\delta}} = \frac{\Lambda(\theta)}{1-\varepsilon\cos(\theta-\alpha+\delta)} \approx \Lambda(\theta)\left[1+\varepsilon\cos(\theta-\alpha+\delta)\right] \quad (5)$$

and

$$\Lambda(\theta) = \Lambda_0\left[1+\sum_{n=0}\lambda_{An}\cdot\cos(nZ\theta)\right] \quad (6)$$

where $Z$ is the number of stator slot, $\lambda_n$ the coefficient of the $n$th order unit permeance of the air-gap, and $\Lambda_0$ the average permeance of the air-gap, which is related with $\varepsilon$. $\Lambda_0$ is also linked with the thickness and permeability of the magnet and the stator slot structure.

Authorized licensed use limited to: University of Shanghai For Science and Technology. Downloaded on July 13,2020 at 12:10:12 UTC from IEEE Xplore. Restrictions apply.

In the motor operation, the magnetic motive force (MMF) generated by the PM ring can be described by

$$F_R(\theta,\alpha)=\sum_{n=0}F_{R2n-1}sin\left[(2n-1)p(\theta+\alpha)\right] \tag{7}$$

where $\theta$ is the position of the field, $p$ the pole-pair of the PM ring, and $\alpha$ rotor phase difference w.r.t. the stator reference point. It is clear that $\alpha$ is a function of time and rotor speed.

Using magnetic-circuit method, the effective magnetic flux density in the air-gap can be expressed as

$$B_A(\theta,\alpha,\delta)=\Lambda_e(\theta,\alpha,\delta)\cdot F_R(\theta,\alpha). \tag{8}$$

The local radial force area density at position $\theta$ can thus be calculated by

$$P_A(\theta,\alpha,\delta)=\frac{1}{2\mu_0}B_A^2(\theta,\alpha,\delta) \tag{9}$$

where $\mu_0$ is the permeability of vacuum.

Therefore, the UMP, $P_A(\alpha,\delta)$, can be calculated by the following:

$$\begin{aligned}P_A(\alpha,\delta)&=\int_0^{2\pi}p_A(\theta,\alpha,\delta)R_A d\theta\\&=\frac{R_A}{2\mu_0}\int_0^{2\pi}B_A^2(\theta,\alpha,\delta)d\theta\\&=\frac{R_A}{2\mu_0}\int_0^{2\pi}\Lambda_e^2(\theta,\alpha,\delta)F_R^2(\theta,\alpha)d\theta\end{aligned} \tag{10}$$

where $R_A$ is the average radius of the air-gap.

From (5) and (7) it can be known that

$$\begin{aligned}\Lambda_e^2(\theta,\alpha,\delta)&=\sum_{m=0}l_{Am}\cdot\cos(mZ\theta)\\&\quad\times\left[1+\varepsilon\cos(\theta-\alpha+\delta)\right]^2\\&\approx\sum_{m=0}l_{Am}\cdot\cos(mZ\theta)\\&\quad\times\left[1+2\varepsilon\cos(\theta-\alpha+\delta)\right]\end{aligned} \tag{11}$$

and

$$F_A^2(\theta,\alpha)=\sum_{n=0}f_{A2n}\cdot\cos\left[2np(\theta-\alpha)\right]. \tag{12}$$

The definitions of $\mathrm{l_{Am}}$ and $\mathrm{f_{An}}$ can be found in [10].

Using the results shown in (11) and (12), the UMP can be deduced as

$$\begin{aligned}P_A(\alpha,\delta)=\frac{R_A}{2\mu_0}\times\int_0^{2\pi}&\left[\sum_{m=0}l_{Am}\cdot\cos(mZ\theta)\right]\\&\cdot\left[1+2\varepsilon\cos(\theta-\alpha+\delta)\right]\\&\times\sum_{n=0}f_{A2n}\cdot\cos\left[2np(\theta-\alpha)\right]d\theta\end{aligned} \tag{13}$$

and

$$\begin{aligned}P_{AI}(\alpha)=\frac{R_A}{2\mu_0}\times\int_0^{2\pi}&\left[\sum_{m=0}l_{Am}\cdot\cos(mZ\theta)\right]\\&\cdot\sum_{n=0}f_{A2n}\cdot\cos\left[2np(\theta-\alpha)\right]d\theta\end{aligned} \tag{14}$$

where $\mathrm{P_{AI}}(\alpha)$ is just the component caused by EM structure reported in [10] as intrinsic UMP.

For the UMP due to rotor misalignment, $\mathrm{P_{AE}}(\alpha,\delta)$ can be expressed as

$$\begin{aligned}P_{AE}(\alpha)=\frac{\varepsilon R_A}{2\mu_0}\times\int_0^{2\pi}&\sum_{m=0}l_{Am}\\&\cdot\left\{cos\left[(mZ+1)\theta-\alpha+\delta\right]\right.\\&\quad\left.+\,cos\left[(mZ-1)\theta-\alpha+\delta\right]\right\}\\&\times\sum_{n=0}f_{A2n}\cdot\cos\left[2np(\theta-\alpha)\right]d\theta.\end{aligned} \tag{15}$$

Therefore, the UMP in $X$ direction can be expressed as

$$\begin{aligned}P_{AE\_X}(\alpha)=\frac{\varepsilon R_A}{2\mu_0}\times\int_0^{2\pi}&\sum_{m=0}l_{Am}\\&\cdot\left\{cos\left[(mZ+2)\theta-\alpha+\delta\right]\right.\\&\quad\left.+\,cos\left[(mZ-2)\theta-\alpha+\delta\right]\right\}\\&\times\sum_{n=0}f_{A2n}\cdot\cos\left[2np(\theta-\alpha)\right]d\theta.\end{aligned} \tag{16}$$

From the orthogonality of the triangular function, it can be known that the integrations of all the items in (15) are zero except the items which can meet the following condition:

$$\begin{cases}2np=mZ\pm2\\2np=mZ\end{cases}. \tag{17}$$

Equation (16) can be simplified as

$$P_{AE\_X}(\alpha,\delta)=\frac{\varepsilon R_A\pi}{2\mu_0}\times CoP_{GE\_X} \tag{18}$$

where

$$\begin{aligned}CoP_{GE\_X}=&\sum_m f_{A2n}l_{Am}\\&\cdot\cos\left[2np\alpha-(\alpha-\delta)\right]|_{2np=mZ+2}\\&+\sum_m f_{A2n}l_{Am}\\&\cdot\cos\left[2np\alpha+(\alpha-\delta)\right]|_{2np=mZ-2}\\&+\sum_m f_{A2n}l_{Am}\\&\cdot\cos\left[2np\alpha-(\alpha-\delta)\right]|_{2np=mZ}\\&+\sum_m f_{A2n}l_{Am}\\&\cdot\cos\left[2np\alpha+(\alpha-\delta)\right]|_{2np=mZ}.\end{aligned} \tag{19}$$

Using the same procedure, the UMP in the $Y$ direction can be obtained and expressed as

$$P_{AE\_Y}(\alpha,\delta)=\frac{\varepsilon R_A\pi}{2\mu_0}\times CoP_{GE\_Y} \tag{20}$$

Authorized licensed use limited to: University of Shanghai For Science and Technology. Downloaded on July 13,2020 at 12:10:12 UTC from IEEE Xplore. Restrictions apply.

where

$$\begin{aligned} CoP_{GE\_Y} = &\sum_m f_{A2n} l_{Am} \\ &\cdot \sin\left[2np\alpha - (\alpha - \delta)\right]|_{2np=mZ+2} \\ &- \sum_m f_{A2n} l_{Am} \\ &\cdot \sin\left[2np\alpha + (\alpha - \delta)\right]|_{2np=mZ-2} \\ &+ \sum_m f_{A2n} l_{Am} \\ &\cdot \sin\left[2np\alpha - (\alpha - \delta)\right]|_{2np=mZ} \\ &- \sum_m f_{A2n} l_{Am} \\ &\cdot \sin\left[2np\alpha + (\alpha - \delta)\right]|_{2np=mZ}. \end{aligned} \quad (21)$$

Equations (18) and (20) are the x and y components of the calculated UMP exerted on the rotor cross section shown in Fig. 7.

For the global radial IUMP of the motor shown in Fig. 4, the eccentricity of any section can be expressed as

$$\varepsilon = \varepsilon_1 + \frac{L}{L_0}(\varepsilon_2 - \varepsilon_1). \quad (22)$$

Substitute (22) into (18) and (20), respectively, integrate (18) and (20) with variable $L$ within $0 \sim \mathrm{L}_0$, and the global IUMP in the $X, Y$ direction can thus be expressed as

$$P_{GE\_X}(\alpha, \delta) = \frac{(\varepsilon_1 + \varepsilon_2) L_0 R_A \pi}{4\mu_0} \times CoP_{GE\_X} \quad (23)$$

and

$$P_{GE\_Y}(\alpha, \delta) = \frac{(\varepsilon_1 + \varepsilon_2) L_0 R_A \pi}{4\mu_0} \times CoP_{GE\_Y}. \quad (24)$$

For the case shown in Fig. 5 where $\varepsilon_1$ is zero, the $\mathrm{P}_{\mathrm{GE\_X}}(\alpha, \delta)$ and $\mathrm{P}_{\mathrm{GE\_Y}}(\alpha, \delta)$ can be calculated as

$$P_{GE\_X}(\alpha, \delta) = \frac{\varepsilon_2 L_0 R_A \pi}{4\mu_0} \times CoP_{GE\_X} \quad (25)$$

and

$$P_{GE\_X}(\alpha, \delta) = \frac{\varepsilon_2 L_0 R_A \pi}{4\mu_0} \times CoP_{GE\_Y}. \quad (26)$$

The IUMP components $\mathrm{P}_{\mathrm{GE\_X}}(\alpha, \delta)$ and $\mathrm{P}_{\mathrm{GE\_Y}}(\alpha, \delta)$, in Fig. 6, however, are more complicated. The relationships among the variables can be expressed as

$$\varepsilon_{01} = \frac{a_1 - L}{a_1}\varepsilon_1, \varepsilon_{02} = \frac{L - a_1}{a_2}\varepsilon_2 \quad (27)$$

and

$$a_1 = \frac{\varepsilon_1}{\varepsilon_1 + \varepsilon_2} L_0. \quad (28)$$

Assume $\varepsilon_2 > \varepsilon_1$, and $\mathrm{P}_{\mathrm{GE\_X}}(\alpha, \delta)$, and $\mathrm{P}_{\mathrm{GE\_Y}}(\alpha, \delta)$ in Fig. 6 can be expressed as

$$\begin{aligned} P_{GE\_X}(\alpha, \delta) = &\left[ -\frac{R_A \pi}{2\mu_0} \int_0^{a_1} \frac{a_1 - L}{a_1} \varepsilon_1 dL \right. \\ &\left. + \frac{R_A \pi}{2\mu_0} \int_{a_1}^{L_0} \frac{L - a_1}{a_2} \varepsilon_2 dL \right] \times CoP_{GE\_X} \\ = &\frac{2L_0^2 - 2a_1 L_0 + a_1^2 - a_1 a_2}{2a_2} \\ &\times \frac{R_A \pi}{2\mu_0} \times CoP_{GE\_X} \\ = &\frac{2\varepsilon_1^2 + \varepsilon_1 \varepsilon_2 + 2\varepsilon_2^2}{2\varepsilon_2} \\ &\times \frac{R_A \pi}{2\mu_0} \times CoP_{GE\_X} \end{aligned} \quad (29)$$

and

$$\begin{aligned} P_{GE\_Y}(\alpha, \delta) = &\left[ -\frac{R_A \pi}{2\mu_0} \int_0^{a_1} \frac{a_1 - L}{a_1} \varepsilon_1 dL \right. \\ &\left. + \frac{R_A \pi}{2\mu_0} \int_{a_1}^{L_0} \frac{L - a_1}{a_2} \varepsilon_2 dL \right] \times CoP_{GE\_Y} \\ = &\frac{2L_0^2 - 2a_1 L_0 + a_1^2 - a_1 a_2}{2a_2} \\ &\times \frac{R_A \pi}{2\mu_0} \times CoP_{GE\_Y} \\ = &\frac{2\varepsilon_1^2 + \varepsilon_1 \varepsilon_2 + 2\varepsilon_2^2}{2\varepsilon_2} \\ &\times \frac{R_A \pi}{2\mu_0} \times CoP_{GE\_Y}. \end{aligned} \quad (30)$$

From the previous results, the following deductions can be obtained.

- *Deduction-1:* IUMP has a constant component in eccentricity direction only.
- *Deduction-2:* In one motor revolution, the lowest order of the IUMP harmonic is two times that of its pole-pair number.
- *Deduction-3:* The orders of the IUMP harmonics are independent of the eccentricity.

## III. Numerical Analysis on IUMP

For verifying the analytical results obtained in Section II, a misalignment PMSM motor is simulated with a 3-D finite element method (FEM), and the FEM results are compared with the analytical ones. The PMSM used has 12 stator slots and 5 magnetic pole-pairs, and its structure is shown in Fig. 8. The motor will be called M1 in the paper. M1 has the rotor with surfaced mounted magnet. Its detailed dimensions are shown in Table I.

In the simulation, the motor is processed with ten segments as illustrated in Fig. 9. The eccentricity ratio and the direction of eccentricity are thus different in each segment. Therefore, the IUMP should be different in each segment and the IUMP center may vary in different segments. In order to calculate the IUMP accurately, the stator is processed to be formed by ten segments in axial direction, and four sections in the $XY$ plane, and they are named Sections A, B, C, and D, respectively.

Authorized licensed use limited to: University of Shanghai For Science and Technology. Downloaded on July 13,2020 at 12:10:12 UTC from IEEE Xplore. Restrictions apply.

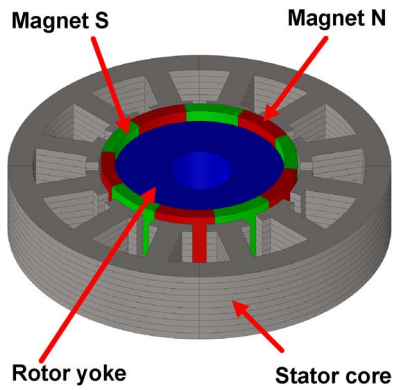


Fig. 8. M1: Spindle motor with 12 slots and 5 magnetic pole-pairs.

TABLE I
DETAIL DIMENSIONS OF SIMULATION MOTOR

| | |
|---|---|
| Rotor core inner diameter | 10mm |
| Rotor core outer diameter | 33.8mm |
| Rotor core width | 13.0mm |
| Magnet inner diameter | 33.8mm |
| Magnet outer diameter | 39.0mm |
| Magnet width | 17.8mm |
| Stator core length | 15.0mm |
| Stator core inner diameter | 66.0mm |
| Stator core outer diameter | 76.0mm |
| Stator core teeth length | 13.0mm |
| Stator core teeth width | 4.8mm |
| Stator core teeth thickness | 15.0mm |

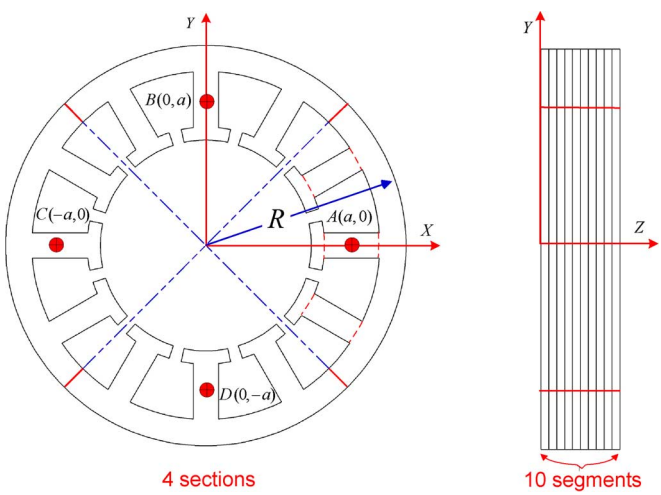


Fig. 9. Divided sections and segments of stator core of M1.

For M1, as its pole-pair is 5 and slot number is 12, using (18) and (23), the following results can be obtained conveniently.

1) IUMP contains constant value component in the x direction when $(\alpha - \delta) = 0$.
2) The lowest order harmonic of the IUMP in the x direction is 10, two times of pole pair, five in this case.
3) The lowest order harmonic of the IUMP in each segment is the same as (10) although eccentricity is different.

Equations (20) and (24) can lead to the following results.

1) IUMP does not contain a constant value component in the y direction when $(\alpha - \delta) = 0$.

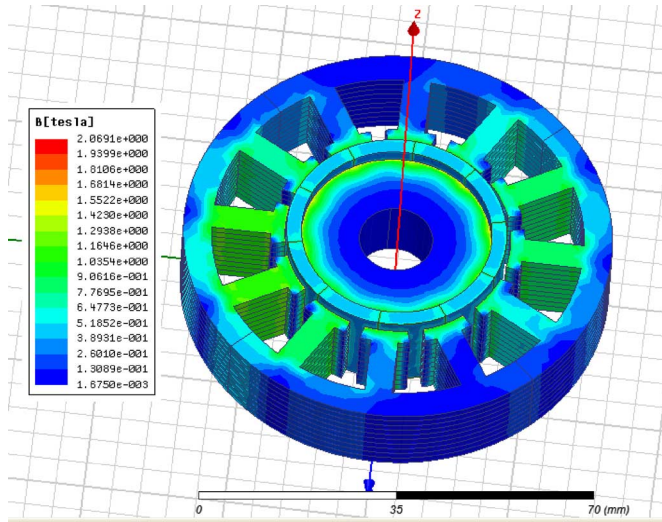


Fig. 10. M1: Magnetic field distribution.

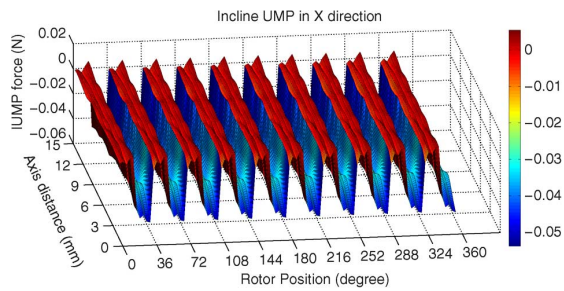


Fig. 11. M1: IUMP in X direction of M1.

2) The lowest order harmonic of the IUMP in the y direction is 10, two times the pole pair, five in this case.

As the geometry of each stator segment is symmetrical with four cycles, it is necessary to calculate only one section in one segment. In Fig. 9, it can be known that the geometry of Section A is symmetric about the x-axis and the x coordinate of the acting point of the IUMP in Section A can be calculated by

$$C_x = \frac{\int_0^R x \cdot y(x) d_x}{\int_0^R y(x) d_x}. \tag{31}$$

Here, it is assumed that the acting point of local UMP of Section A is at (a,0). Because of the symmetrical structure of the stator, the action points of Sections B, C, and D are (0,a), (-a,0), and (0,-a), respectively. After the UMP in each segment is obtained by ANSOFT, the total UMP in one section can be calculated. Fig. 10 shows the magnetic field distribution of PMSM obtained with Maxwell 3-D static magnetic solver. From the analytical analysis in Section II, the order of fundamental harmonic of the UMP in space domain is 10, which is the same as the numerical results obtained with FEM shown in Figs. 11–13.

Fig. 11 shows the IUMP component in the x direction, which is obtained with 3-D FEM. It can be found in the figure that the frequency of the x component is also ten times that of rotor rotating frequency, which is still the same as the one estimated with the analytical model in Section II.

DC offset of IUMP can be found in Fig. 11. The reason is that the incline eccentricity is also a type of rotor static eccentricity. This result confirms the one obtained by using the analytical

Authorized licensed use limited to: University of Shanghai For Science and Technology. Downloaded on July 13,2020 at 12:10:12 UTC from IEEE Xplore. Restrictions apply.

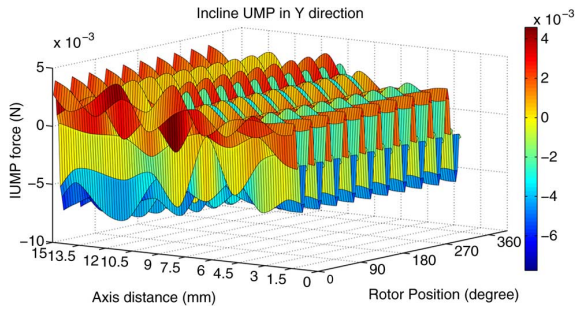


Fig. 12. M1: IUMP in Y direction.

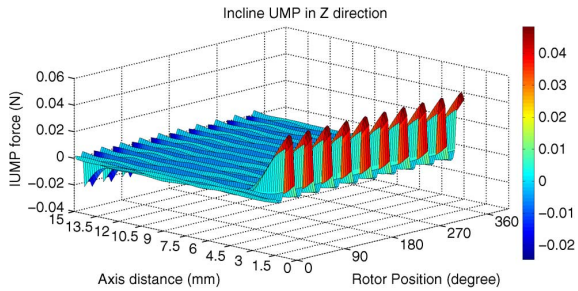


Fig. 13. M1: IUMP in Z direction.

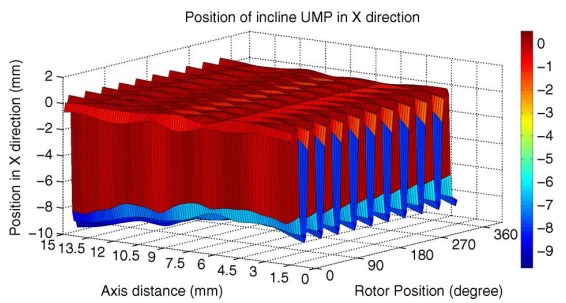


Fig. 14. M1: Variation of acting point of IUMP in x direction.

model shown in (18) when $(\alpha - \delta)$ is zero (refer to Fig. 7). It can also be found that the lowest order harmonic of the IUMP in all ten segments is the same and is ten times that of rotor rotating frequency.

Fig. 12 shows the IUMP component in y direction. Though there is not any incline eccentricity in the y direction, IUMP in the y direction still exits and its frequency is also ten times that of rotor rotating frequency. But, comparing its x component, the IUMP component in the y direction is quite small. Fig. 12 shows also that the IUMP in the y direction does not have any dc offset, which is also the same as the one estimated in Section II.

Fig. 13 shows the IUMP component in the z direction. It can be found that, besides the frequency being ten times that of rotor speed, the local IUMP at the end segment in the Z direction is larger than that in the middle section of the stator. This phenomenon is caused by the end point angular effect of the misalignment axis.

In Figs. 14 and 15, it can be seen that besides the variations of the direction and amplitude, the acting point of IUMP also

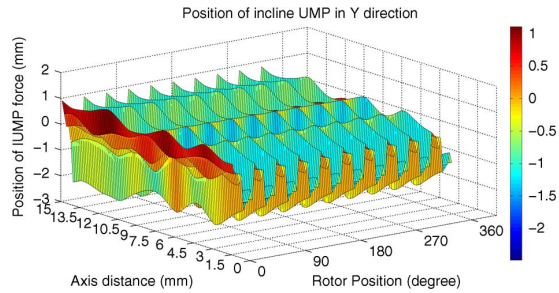


Fig. 15. M1: Variation of acting point of IUMP in y direction.

changes during motor operation, which would certainly cause additional motor vibration and acoustic noise. As a result, the RRO and NRRO of the motor would also be increased.

## IV. Conclusion

The IUMP may induce serious vibration, acoustic noise and run out in the motor operation. However, the influences of the IUMP have not been well studied in many applications. This paper presents an analytical model to analyze this kind of UMP. The analysis shows clearly that the acting point of IUMP varies at the frequency which is the fundamental rotating frequency times the number of motor magnetic poles. The deductions through the analytical model have been confirmed by the numerical results, and they can thus be used to analyze high performance PMSM and can also be used in motor misalignment failure diagnosis.

## References

[1] C. Bi, N. L. H. Aung, H. N. Phyu, Q. Jiang, and S. Lin, "Unbalanced magnetic pull induced by drive current in PM-BLDC motor operation," in *Proc. ICEMS-2007*, Seoul, Korea, Oct. 8–11, 2007.

[2] S. Lin, Q. Jiang, A. A. Mamun, and C. Bi, "Effect of drive modes on the acoustic noise of fluid dynamic bearing spindle motors," *IEEE Trans. Magn.*, vol. 39, no. 5, pt. 2, pp. 3277–3279, Sep. 2003.

[3] S. Rajagopalan, "Dynamic eccentricity and demagnetized rotor magnet detection in trapezoidal flux (brushless DC) motors operating under different load conditions," *IEEE Trans. Power Electron.*, vol. 22, no. 5, Sep. 2007.

[4] B. M. Ebrahimi, M. Etemadrezaei, and J. Faiz, "Dynamic eccentricity fault diagnosis in round rotor synchronous motors," *Energy Conversion Manage.*, vol. 52, pp. 2092–2097, 2011.

[5] C. Bi, N. L. H. Aung, Q. Jiang, and S. Lin, "Influence of rotor eccentricity to unbalanced-magnetic-pull in PM synchronous motor," in *Proc. ICEMS06*, Nagasaki, Japan, Nov. 20–23, 2006.

[6] U. Werner, "Theoretical analysis of shaft vibrations in two-pole induction machines considering static rotor eccentricity," in *Proc. Int. Symp. Power Electronics, Electrical Drives, Automation and Motion, SPEEDAM, 2010*.

[7] [Online]. Available: http://www.nbcgroup.co.uk/bearings

[8] J. R. Hendershot and T. J. E. Miller, *Design of Brushless Permanent-Magnet Motors*. Oxford, MA, USA: Oxford Univ. Press, Jun. 15, 1995.

[9] K. J. Binns, W. R. Barnard, and M. A. Jabbar, "Hybrid permanent-magnet synchronous motors," *Proc. IEE*, vol. 125, no. 3, Mar. 1978.

[10] C. Bi, Q. Jinang, and S. Lin, "Unbalanced-magnetic-pull induced by the EM structure of PM spindle motor," in *Proc. ICEMS05*, Nanjing, China, Sep. 26–29, 2005.

Authorized licensed use limited to: University of Shanghai For Science and Technology. Downloaded on July 13,2020 at 12:10:12 UTC from IEEE Xplore. Restrictions apply.